Vorticity statistics in the near wake of asymmetric prismatic airfoil NACA 64-618 at negative angle of attack –10° at Reynolds numbers $1.6 \cdot 10^4$ and $1.6 \cdot 10^5$ in distance 0.0 – 0.4 × chord past trailing edge measured by Particle Image Velocimetry

Jan Narovec[1], *Daniel* Duda[1*], *Vít* Horáček[1], *Tetjana* Tomášková[1], *Václav* Uruba[1,2], *Vitalii* Yanovych[1,2]

[1]Faculty of Mechanical Engineering, University of West Bohemia in Pilsen, Univerzitní 22, 306 14, Pilsen, Czech Republic
[2]Institute of Thermomechanics, Czech Academy of Sciences, Dolejškova 5, 180 00, Prague, Czech Republic

Abstract. The airfoil NACA 64-618 is realized by using two levels of quality: first the theoretical profile is printed on a 3D printer in a direct, "naive" way, this geometry has been scanned by using 3D scanner and based on the deviations, a better model has been processed. The flow within the turbulent wake is measured by using Particle Image Velocimetry (PIV) technique at two velocities separated by one order of magnitude.

1 Introduction

Vorticity is a local derivative invariant of velocity field $\vec{u}$ defined as [1]

$$\vec{\omega} = \nabla \times \vec{u}\,, \qquad \text{i. e. } \omega_i = \epsilon_{ijk} \frac{\partial u_j}{\partial x_k} \tag{1}$$

where ∇ is spatial gradient vector operator, $\times$ is vector product, therefore vorticity is, correctly speaking, *pseudovector*, thus in two dimensions, it is a scalar (1D) field, while in four dimensions, it would be a second order tensor with 6 independent components. Only in 3D space, number of its independent components matches the dimension. The more exact expression calls the total antisymmetric *Levi-Civita tensor* ϵ_{ijk}. Vorticity is invariant in respect to Galilean transformation and it can be used to eliminated pressure from the Navier-Stokes equations (NSE), however, it is not possible to solve NSE with vorticity only, as the vorticity itself is advected by velocity field [1].

The term "vorticity" is little bit misleading, as presence of vorticity does not proof existence of vortex in a such coordinate. E.g. shear flow displays nonzero vorticity, although there is no vortex and oppositely, there is zero vorticity in a vortex envelope.

* Corresponding author: dudad@kke.zcu.cz

2 Experimental setup

2.1 Airfoil printing and scanning

A pair of airfoil realizations is compared here. The first one is created by "naive" approach: download coordinates from public database [2] and print by using a commercial 3D printer Prusa Mk2.5 from PLA [3]. The GOM Atos 3D scanner [4] [5] [6] is used to measure the shape and to compare with the design. The largest discrepancy is found at the thin trailing edge, which is not printed correctly and is shorter. The second, "processed", variant gains from the errors observed in the first case, thus its trailing edge is slightly remodeled and the surface is smoother by using sandpaper. Additionally, the surface roughness R_q and roughness high R_t is measured by using device Taylor Hobson Sulfronic Duo.

Tab. 1 Basic parameters the studied airfoil realizations compared with the ideal design

	Chord [mm]	Thickness [mm]	Roughness high R_t [μm]	Roughness R_q [μm]
Design	80.00	14.36	0.0	0.0
Naïve	77.01	14.34	70.5	11.35
Processed	80.08	14.47	60.1	9.77

2.2 PIV measurement system

Particle Image Velocimetry (PIV) [7] system at the University of West Bohemia (UWB) is a standard one supplied by the Dantec company. It consists of pair of FlowSense MkII cameras with resolution of 4 MPix, solid-state double pulse laser New Wave Solo with emitting energy of 0.5 J during 5 ns pulse (i.e. power during pulse is around 100 MW). The tracer particles are very small droplets made by fog generator Safex by using liquid of unknown composition. The dimension of the droplets has not been measured, but its usage is proved by wide experience with this method [7]. The system takes a pair of photos separated by time 100 μs (for $\mathrm{Re} = 1.6 \cdot 10^4$) or 10 μs (for $\mathrm{Re} = 1.6 \cdot 10^5$) respectively. The repeating frequency of these pairs is 7.4 Hz. Data acquisition is performed by Dantec Dynamic Studio. 2D velocity vector field is calculated by using the "Adaptive PIV" function built in the Dantec Dynamic Studio. The post-processing is made by custom-made software.

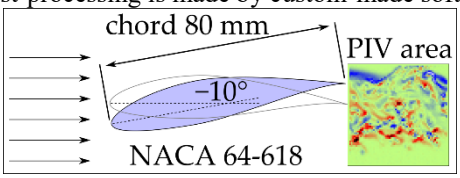

Fig. 1. Sketch of the airfoil profile with measured PIV area.

3 Results

3.1 Statistical moments of vorticity

Figure 2 shows the example of few instantaneous data and the mean vorticities in the four discussed cases. The airfoil realizations are denoted "naive", or case A in our work [8], and "processed", or case C in [8]. We see that both realization display similar topology at same Reynolds numbers, while the Reynolds number (controlled via velocity) has much stronger

effect on the mean wake shape. At lower Re, the flow is separated at the leading edge forming a massive wake structure covering the entire Field of View (FoV). At higher Re, the flow is attached, the wake is much narrower, but still a strong asymmetry between pressure (bottom in figures) and suction sides can be observed.

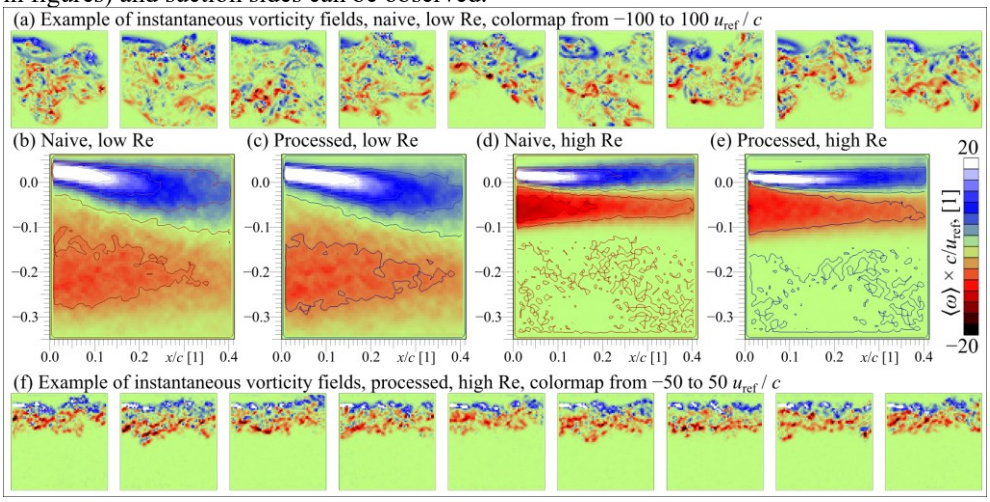

Fig. 2. Vorticity maps. Top line (a) shows examples of instantaneous in-plane vorticity maps measured past the "naive" realization of airfoil, the better realization is too similar to observe differences in instantaneous fields. Middle line (b – e) shows the mean vorticity maps in all discussed cases, low Re = · 10^4, high Re = 1.6 · 10^5. Interval between isolines is 5. The bottom line (f) shows examples of instantaneous vorticities past the better processed airfoil at higher Re.

The standard deviation field is calculated as

$$\sigma_\omega(\vec{x}) = \sqrt{\langle\omega(\vec{x})^2\rangle - \langle\omega(\vec{x})\rangle^2} \tag{2}$$

where $\langle\omega\rangle$ plays for ensemble average over the measured snapshots (whose number is 650). The second power of standard deviation is sometimes referred as *Enstrophy*, but the correct enstrophy needs all three component of vorticity variance, while the 2D PIV measurement can offer only the component perpendicular to the measured plane. Figure 3 shows a pair of high-activity strips in the airfoil wake – top one behind the suction side and the bottom one behind the pressure side, where the bottom one is weaker and more diffused. At higher Re, weaker fluctuations can be observed behind the processed airfoil (Fig. 3c vs. Fig. 3d).

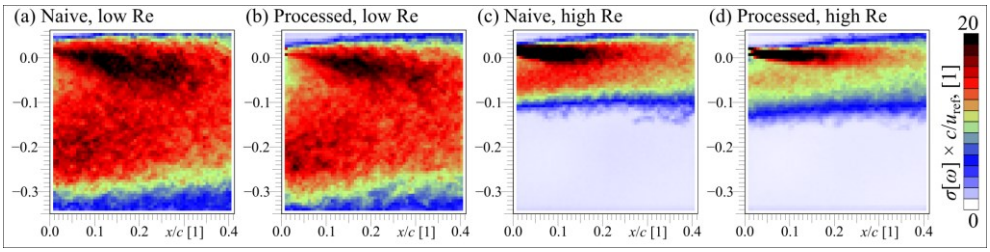

Fig. 3. Maps of standard deviation of vorticity past both discussed airfoil realizations and at both discussed Reynolds numbers.

The *skewness* (or *asymmetry coefficient* or *3rd statistical moment*, česky *koeficient šikmosti*) is calculated as

$$S_\omega(\vec{x}) = \frac{\langle\omega'^3(\vec{x})\rangle}{\sigma_\omega^3(\vec{x})} \tag{3}$$

where the prime denotes fluctuation components, i.e. $\omega'(\vec{x}) = \omega(\vec{x}) - \langle\omega(\vec{x})\rangle$. In the case of symmetric distribution, the skewness is zero. The positive skewness means, that there is lower number of stronger positive events, while the negative events are weaker and of higher amount. The negative skewness does oppositely. In the case of wake, the vortices can be ejected into the corresponding boundary more easily than to the other side. Therefore, the wake is bounded by the sharp cliff of skewness in the most distant area, in which a vortex can be ejected. This property can be used as a wake boundary [9].

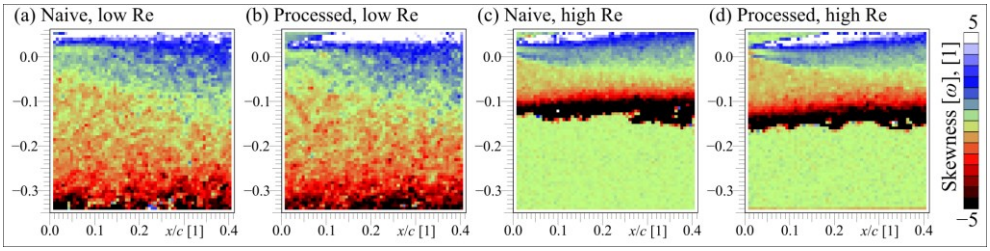

Fig. 4. Maps of skewness (i.e. third statistical moment, sometimes asymmetry coefficient) of vorticity past both discussed airfoil realizations and at both discussed Reynolds numbers.

The *flatness* (or *4th statistical moment* or *kurtosis*, česky *koeficient špičatosti*) is

$$F_\omega(\vec{x}) = \frac{\langle\omega'^4(\vec{x})\rangle}{\sigma_\omega^4(\vec{x})} \tag{4}$$

Its value is always positive and it can be proven, that the flatness of Gauss distribution is equal to 3 (pure red color in Fig. 5), while the flatness of any distribution with polynomial tails diverges [10]. Physical interpretation is, that higher flatness signifies occurrence of strong rare events. Typically, at the wake boundary, there is generally quiet flow, which is time-to-time visited by a vortex from the shear layer region. Such events increase the standard deviation only little, while its effect on flatness is strong. In the central part of the wake, the vorticity flatness is slightly higher than 3. Its expected value for homogenous turbulence is not known, but it has been observed, that in grid-generated turbulence, the vorticity flatness lies between 3 and 4.5 with increase with increasing Re [11], but current results suggest higher flatness at lower Re; however it is questionable, if it can be compared, when the flow state is different.

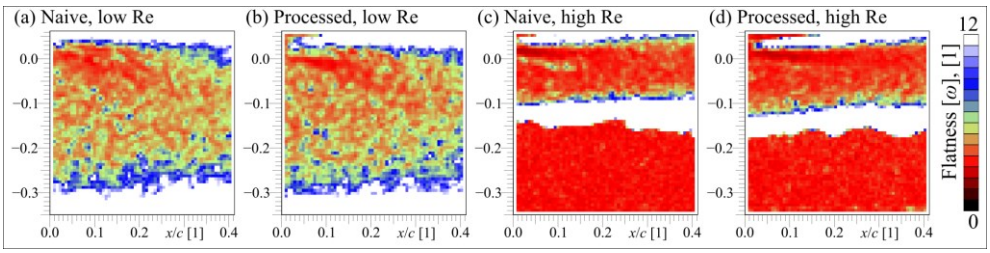

Fig. 5. Maps of flatness of vorticity field convoluted by Gaussian function of width $\sigma = 0.007c$ past both discussed airfoil realizations and at both discussed Reynolds numbers. The pure red corresponds to the value of 3.

3.2 Spectral dependence

Alexakis & Biferale [12] discuss the spectral flux of energy and enstrophy. Unfortunately, the flux is invisible by using our equipment with low time resolution. The change of sign in the energy and enstrophy flux correspond to the transition between direct and indirect cascade

at the integral lengthscale. The current studied flow is 3D, but the geometry is prismatic, hence there can be expected 2D behaviour (of course, it has been proven by Wilkinson [13] and others [14] in nineteens, that cylinder perpendicular to the flow produces fully 3D flow since very small Reynolds numbers). However, it has been observed by Solís-Gallego [15] and later confirmed by us [16], that the flow behind prismatic airfoil exhibits two slope energy spectrum similarly as some 2D flows do (e.g. the atmosphere of Earth and Venus [17]). The best we can do with our current data in this direction is to explore the spectral dependence of vorticity statistics, mainly its standard deviation, which relates to enstrophy.

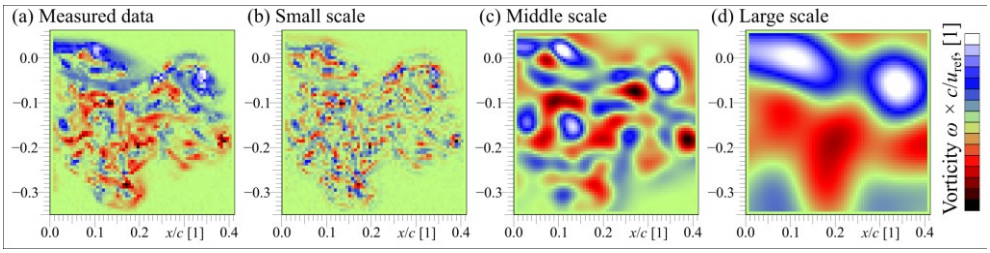

Fig. 6. Example of single instantaneous snapshot (a) decomposed into three length-scale intervals (b-d). The "small scale" corresponds to lengths 0.006 – 0.010 c, "middle scale" means 0.020 – 0.027 c and the "large scale" denotes fluctuations of sizes 0.05 – 0.08 c. the limits of colormap are different for each panel adapting the actual values.

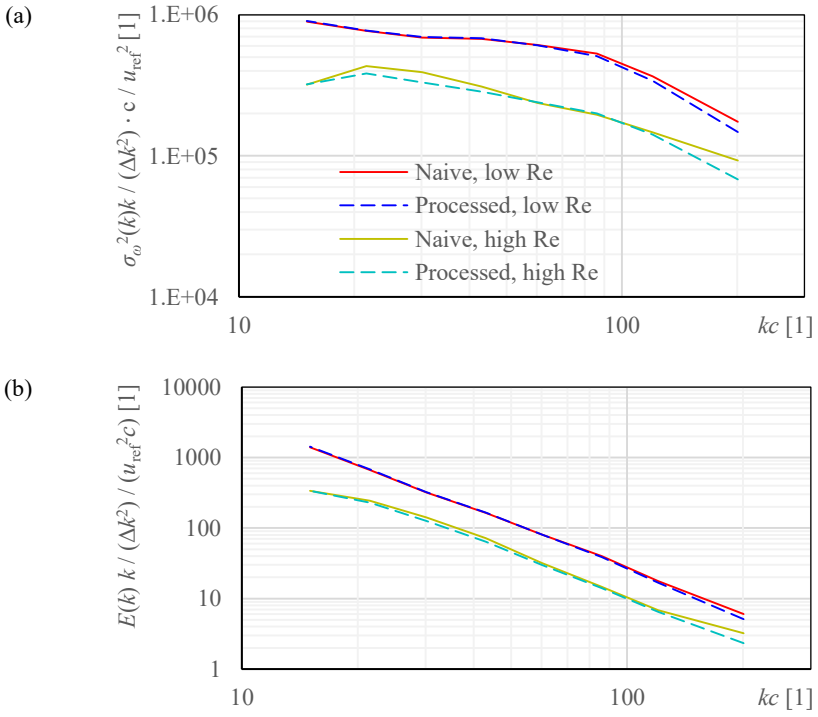

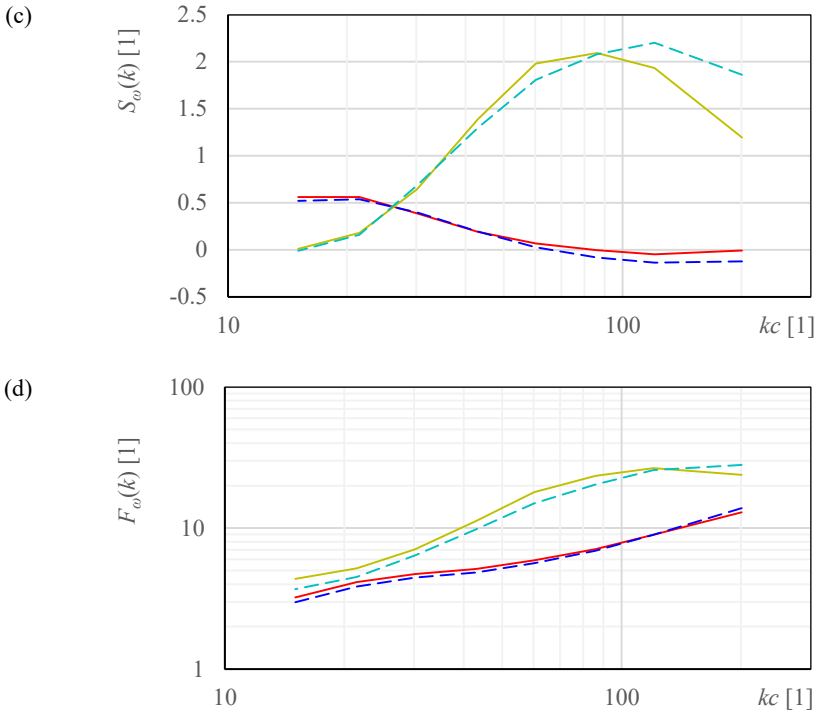

Fig. 7. Spectral dependence of selected quantities. (a): vorticity variance (σ^2) as a function of wavenumber k. (b) power spectral density. (c) vorticity skewness S_ω as a function of wavenumber. (d): vorticity flatness F_ω. Solid red line: naïve at lower Re, dashed blue: processed at lower Re, solid yellow: naïve at higher Re, dashed azure: processed at higher Re.

The decomposition to different lenghtscales is done by using consecutive convolutions with band-pass filters

$$P[\sigma_h, \sigma_l](\xi) = \frac{\exp\left(-\frac{\xi^2}{2\sigma_l}\right)}{2\pi\sigma_l} - \frac{\exp\left(-\frac{\xi^2}{2\sigma_h}\right)}{2\pi\sigma_h} \tag{5}$$

with σ_l and σ_h spanning the range of PIV data (i.e. from the single grid point 0.5 mm to the field of view 34 mm). More details about this method can be found in our work [18]. Figure 6 shows this decomposition to three lengthscales.

The spectral dependence of vorticity fluctuations is plotted in Fig. 7 top left. It is normalized in a similar manner as the standard power spectral densities (Fig. 7 top right), i.e. the variance (second power of σ) at probed wavenumber k is multiplied by k and divided by the square of the band width Δk, more details in [18]. There is an increasing tendency with lengthscale, which does not seem to follow some simple scaling law. At larger Reynolds number, there is decrease at largest scales (smallest k) as the wake width is smaller in that case. The lower occupied area is also responsible for generally lower values at higher Re (normalization by velocity). The spatial distribution in Fig. 8 shows very similar topology as at all scales (Fig. 3) at small and middle scales, while the large scales fluctuation can emerge only since certain distance past trailing edge (lower Re, Fig. 8 ch, i), or it cannot live in wake smaller than its scale (Fig. 8 j, k).

Surprisingly, the skewness shows very different behaviour at different Reynolds numbers: the decreasing tendency with k switches to increasing tendency at higher velocity. The processed airfoil exhibits larger difference between the begin and end of the probed

lengthscale interval. The vorticity flatness originates at small scales and this effect is stronger at higher velocity. Again, this effect is stronger at processed airfoil, although it displays lower vorticity fluctuations than the unprocessed naïve airfoil realization.

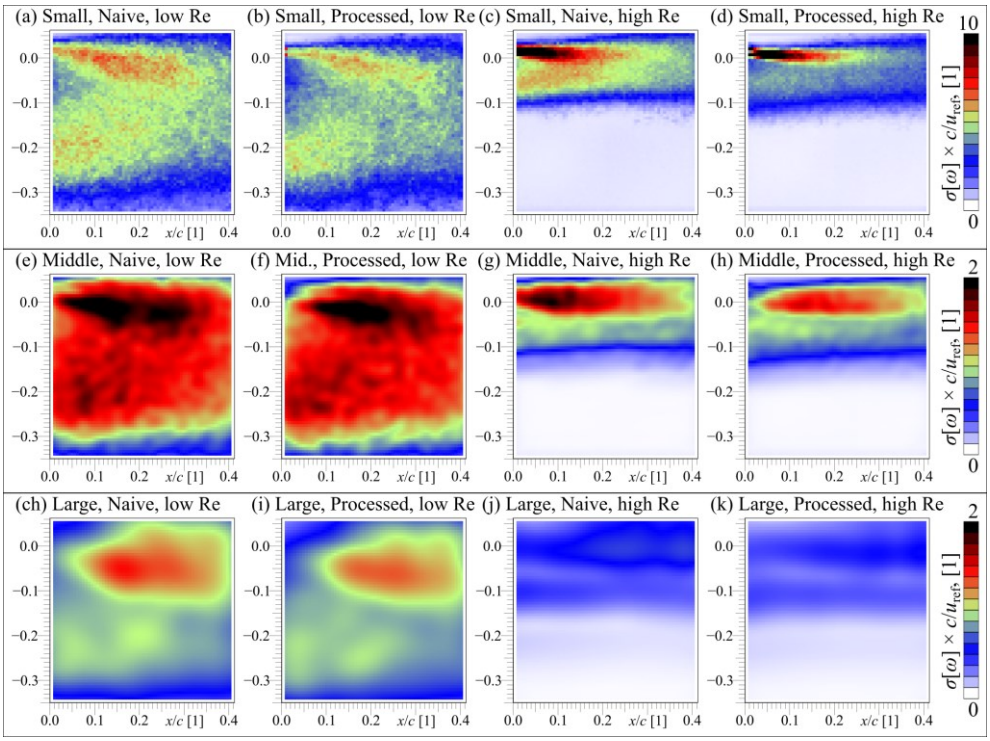

Fig. 8. Scale-dependent standard deviation of vorticity. Top row displays the smallest scales, middle row the middle scale (i.e. 0.020 – 0.027 c) and bottom row shows the vorticity fluctuations at larger scales. The colormap range keeps within each row, while it changes among rows, hence look to Fig. 7 for comparing values.

4 Conclusion

A pair of airfoil realizations is compared, the first one is created by "naive" approach: download coordinates and print, while the "processed" variant gains from the errors observed in the first case, thus its trailing edge is slightly remodeled and the surface is smoother by using sandpaper. Both airfoils produce massive separation at Reynolds number $1.6 \cdot 10^4$, while at higher Re $1.6 \cdot 10^5$ the flow is attached and the wake is more concentrated. The processed airfoil produces smaller vorticity fluctuations, mainly at small scales. The skewness and flatness of vorticity originate at the boundary of the wake. The flatness is produced by small-scale fluctuations, while this source changes with Reynolds number for skewness.

Acknowledgments

The work was supported from ERDF under project "Research Cooperation for Higher Efficiency and Reliability of Blade Machines (LoStr)" No. CZ.02.1.01/0.0/0.0/16_026/0008389.

References

[1] J.-Z. Wu, H.-Y. Ma and M.-D. Zhou, Vorticity and Vortex dynamics, Berlin Heidelberg New York: Springer, 2006.

[2] "Airfoiltools.com," [Online]. Available: http://www.airfoiltools.com/airfoil/details?airfoil=naca643618-il.

[3] S. Inkinen, M. Hakkarainen, A. Albertsson and A. Södergård, "From lactic acid to poly(lactic acid) (PLA): Characterization and analysis of PLA and Its precursors," *Biomacromolecules,* vol. 12, no. 3, pp. 523-532, 2011.

[4] S. Zhang, Handbook of 3D Machine Vision: Optical Metrology and Imaging, Boca Raton: CRC Press, 2013.

[5] J. Vagovský, I. Buranský and A. Görög, "Evaluation of measuring capability of the optical 3D scanner," *Procedia Engineering,* vol. 100, pp. 1198-1206, 2015.

[6] V. Yanovych, D. Duda, V. Uruba and T. Tomášková, "Hot-Wire Investigation of Turbulence Topology behind Blades at Different Shape Qualities," *Processes,* vol. 10, no. 3, p. 522, 2022.

[7] C. Tropea, A. Yarin and J. Foss, Springer Handbook of Experimental Fluid Mechanics, Berlin: Springer, 2007.

[8] D. Duda, V. Yanovych, V. Tsymbalyuk and V. Uruba, "Effect of Manufacturing Inaccuracies on the Wake Past Asymmetric Airfoil by PIV," *Energies,* vol. 15, no. 3, p. 1227, 2022.

[9] D. Duda, V. Uruba and V. Yanovych, "Wake Width: Discussion of Several Methods How to Estimate It by Using Measured Experimental Data," *Energies,* vol. 14, no. 15, p. 4712, 2021.

[10] M. La Mantia, P. Švančara, D. Duda and L. Skrbek, "Small-scale universality of particle dynamics in quantum turbulence," *Physical Review B,* vol. 94, p. 184512, 2016.

[11] D. Duda, V. Yanovych and V. Uruba, "An Experimental Study of Turbulent Mixing in Channel Flow Past a Grid," *Processes,* vol. 8, no. 11, p. 1355, 2021.

[12] A. Alexakis and L. Biferale, "Cascades and transitions in turbulent flows," *Physics Reports,* Vols. 767-769, no. 12, pp. 1-101, 2018.

[13] C. Williamson, "Three-dimensional wake transition," *Journal of fluid mechanics,* vol. 328, pp. 345-407, 1996.

[14] M. Thompson, K. Hourigan and J. Sheridan, "Three-dimensional instabilities in the wake of a circular cylinder," *Experimental Thermal and Fluid Science,* vol. 12, no. 2, pp. 190-196, 1996.

[15] I. Solís-Gallego, A. Meana-Fernández, J. Fernández Oro, K. Argüelles Díaz and S. Velarde-Suárez, "Turbulence Structure around an Asymmetric High-," *Journal of Applied Fluid Mechanics,* vol. 10, no. 4, pp. 1013-1027, 2017.

[16] V. Yanovych, D. Duda, V. Uruba and P. Antoš, "Anisotropy of turbulent flow behind an asymmetric airfoil," *SN Applied Sciences,* vol. 3, p. 885, 2021.

[17] M. Izakov, *Solar System Research,* vol. 47, no. 3, pp. 170-181, 2013.

[18] D. Duda and V. Uruba, "Spatial spectrum from particle image velocimetry data," *Journal of Nuclear Engineering and Radiation Science,* vol. 5, no. 3, pp. 030912-1-030912-7, 2019.